Commun. Comput. Phys.
doi: 10.4208/cicp.271011.020212s

Vol. **13**, No. 3, pp. 671-684
March 2013

# Sound Propagation Properties of the Discrete-Velocity Boltzmann Equation

Erlend Magnus Viggen*

*Department of Electronics and Telecommunications, Norwegian University of Science and Technology (NTNU), 7034 Trondheim, Norway.*

Received 28 October 2011; Accepted (in revised version) 2 February 2012

Available online 29 August 2012

**Abstract.** As the numerical resolution is increased and the discretisation error decreases, the lattice Boltzmann method tends towards the discrete-velocity Boltzmann equation (DVBE). An expression for the propagation properties of plane sound waves is found for this equation. This expression is compared to similar ones from the Navier-Stokes and Burnett models, and is found to be closest to the latter. The anisotropy of sound propagation with the DVBE is examined using a two-dimensional velocity set. It is found that both the anisotropy and the deviation between the models is negligible if the Knudsen number is less than 1 by at least an order of magnitude.

**AMS subject classifications**: 76Q05, 76P05

**Key words**: Lattice Boltzmann method, discrete-velocity Boltzmann equation, sound propagation, computational aeroacoustics.

## 1 Introduction

The lattice Boltzmann method (LBM) is a fairly recent development in computational fluid dynamics (CFD). While traditional CFD methods are based on discretising the conservation equations of the continuum model, the LBM is based on discretising the Boltzmann equation from the kinetic theory of gases. The Boltzmann equation describes how distributions of particles in a gas propagate and collide, thus giving a more detailed picture than the continuum model. It can be shown that the total behaviour of these particle distributions at long time scales corresponds with the conservation equations of the continuum model [1].

Although the lattice Boltzmann method can be used to simulate weakly compressible flow [2], current research has largely been confined to incompressible flow. However, in

*Corresponding author. *Email address:* erlend.viggen@ntnu.no (E. M. Viggen)

 

the last few years several articles have been published on applying the LBM for computational aeroacoustics (CAA) [3, 4], i.e. for simulating generation of sound waves in unsteady flow. This subject is based on the theory of aeroacoustics first developed by Lighthill [5].

In some cases the generated sound has a strong feedback interaction with the fluid flow, as in the problem of tone generation in corrugated pipes [6]. These cases must be studied using a compressible flow simulation. As the LBM is more straightforward to implement and more parallelisable than traditional compressible CFD methods, it could be a useful supplement to traditional CAA methods.

However, the propagation of sound waves for the LBM has not yet been sufficiently studied. A previous article by this author looked at the case of plane sound waves in the LBM [7], and showed disagreement between the LBM and Navier-Stokes even in the limit of no discretisation error. The goal of the present article is twofold: To explain this disagreement, and to further examine the behaviour of the LBM in this limit. The focus here will be narrower than in the previous article; this article will only look at absorption and dispersion of spatially damped plane sound waves.

The limit of no discretisation error is an important one; if a numerical method does not behave correctly in this limit it is inconsistent, and its behaviour can not necessarily be improved by improving the numerical resolution.

In Section 2, the basics of damped plane sound waves are explained. Section 3 derives an analytic expression for the propagation of these sound waves from the discrete-velocity Boltzmann equation (DVBE), which corresponds to the aforementioned limit of the LBM. This is compared in Section 4 with similar expressions from other models. Section 5 extends the derivation from Section 3 to two dimensions, and examines the isotropy properties of the DVBE.

## 2 Damped sound waves

In a sound wave, the density $\rho$, particle velocity $\mathbf{u}$, and pressure $p$ oscillate around an equilibrium state. We assume here that the oscillations are infinitesimal monofrequency plane waves propagating in the $+x$-direction, and write them in phasor form,

$$\begin{bmatrix}\hat{\rho}(x,t)\\ \hat{u}(x,t)\\ \hat{p}(x,t)\end{bmatrix} = \begin{bmatrix}\rho_0\\ 0\\ p_0\end{bmatrix} + \begin{bmatrix}\hat{\rho}'\\ \hat{u}'\\ \hat{p}'\end{bmatrix} \mathrm{e}^{\mathrm{i}(\hat{\omega}t-\hat{k}x)}. \tag{2.1}$$

Throughout this article, hats indicate complex numbers and primes are used for infinitesimally small oscillation amplitudes.

If we split the angular frequency $\hat{\omega}$ and wavenumber $\hat{k}$ into real and imaginary parts,

$$\hat{\omega} = \omega_\mathrm{r} + \mathrm{i}\alpha_t, \qquad \hat{k} = k_\mathrm{r} - \mathrm{i}\alpha_x, \tag{2.2}$$

we find that the real parts govern the wave's propagation, while the imaginary parts govern its absorption,

$$e^{i(\hat{\omega}t-\hat{k}x)}=e^{i(\omega_r t-k_r x)}\,e^{-\alpha_t t}\,e^{-\alpha_x x}.$$

We call $\alpha_t$ and $\alpha_x$ the *temporal* and *spatial absorption coefficients*. The real parts determine the wave's *phase speed*,

$$c=\omega_r/k_r. \tag{2.3}$$

In the low-frequency limit or in an ideal medium with no absorption, $\hat{\omega}$ and $\hat{k}$ are real, and the speed of sound is

$$c_0=\omega/k. \tag{2.4}$$

In general, $\hat{\omega}$ and $\hat{k}$ are determined by initial and boundary conditions. Most commonly, a sound wave is emitted by an oscillating source. In this case, the boundary conditions dictate that $\hat{\omega}$ is real, and thus the degree of absorption only depends on the medium and the distance to the source. The opposite case, where $\hat{k}$ is real and the absorption occurs in time, has recently been examined numerically with both basic isothermal and multispeed thermal LB models [8].

Away from boundaries, there are three causes of sound wave absorption and dispersion: Viscosity, thermal conduction, and relaxation between translational energy and other forms of internal energy [9]. In the basic LBM, the simulated fluid is isothermal. It only has translational internal energy, and is thus comparable to a monatomic gas, where there is no rotational or vibrational molecular energy. Therefore we are left with only the influence of viscosity.

As shown in previous literature [10], the influence of viscosity on a sound wave can be described using the dimensionless *viscosity number*,

$$\omega\tau_\nu=\frac{\omega}{c_0^2}\left(\frac{4}{3}\nu+\nu_B\right). \tag{2.5}$$

where $\nu$ and $\nu_B$ are the kinematic shear and bulk viscosities. While monatomic gases normally have $\nu_B=0$, the isothermal nature of the simulated fluid causes a nonzero $\nu_B$ [2].

To find the sound wave absorption and dispersion, it is sufficient to find the normalised wavenumber $\hat{k}/k=\hat{k}/(\omega/c_0)$. The real part gives the dispersion, and the imaginary part gives the absorption. We will see that $\hat{k}/k$ will be a function only of $\omega\tau_\nu$ for the fluid described above.

When comparing different expressions for $\hat{k}/k$, it will be useful to write them as series expansions around $\omega\tau_\nu=0$,

$$\frac{\hat{k}}{k}=1+a_1(\omega\tau_\nu)+a_2(\omega\tau_\nu)^2+a_3(\omega\tau_\nu)^3+a_4(\omega\tau_\nu)^4+\cdots.$$

It was previously shown that the LBM disagrees with the continuum model, which we will be calling the Navier-Stokes model, above order $\mathcal{O}(\omega\tau_\nu)$ [7].

## 3 Wavenumbers from the discrete-velocity Boltzmann equation

The Boltzmann equation describes the evolution of the distribution function $f(\mathbf{x},\boldsymbol{\xi},t)$, which represents the density of particles with position $\mathbf{x}$ and velocity $\boldsymbol{\xi}$ at time $t$. The first step in discretising the Boltzmann equation is to restrict $f$ to a discrete set of velocities $\boldsymbol{\xi}_i$. We can then rewrite $f(\mathbf{x},\boldsymbol{\xi}_i,t)$ as $f_i(\mathbf{x},t)$.

Macroscopic physical quantities can be found as moments of the distribution function. Density is found as $\rho=\sum_i f_i$, momentum as $\rho\mathbf{u}=\sum_i \boldsymbol{\xi}_i f_i$, and the momentum flux tensor as $\boldsymbol{\Pi}=\sum_i \boldsymbol{\xi}_i\boldsymbol{\xi}_i f_i$.

Having discretised the velocities, the Boltzmann equation becomes the *discrete-velocity Boltzmann equation* (DVBE),

$$\frac{\partial f_i}{\partial t}+\boldsymbol{\xi}_i\cdot\nabla f_i=-\frac{1}{\tau}\left(f_i-f_i^{(0)}\right). \tag{3.1}$$

Here we have the common BGK collision operator on the right-hand side, which describes particle collisions as a relaxation, with characteristic time $\tau$, to an equilibrium. The equilibrium distribution is

$$f_i^{(0)}=\rho w_i\left(1+\frac{\boldsymbol{\xi}_i\cdot\mathbf{u}}{c_0^2}+\frac{(\boldsymbol{\xi}_i\cdot\mathbf{u})^2}{2c_0^4}-\frac{\mathbf{u}^2}{2c_0^2}\right). \tag{3.2}$$

The weighting coefficients $w_i$ are chosen to satisfy certain symmetry conditions of the velocity set [11], so that physically correct collision behaviour, such as conservation of mass and momentum, is ensured.

The DVBE is discrete in velocity, but still continuous in time and space. To go from it to the fully discrete lattice Boltzmann equation which can be implemented on a computer, (3.1) can be integrated along its characteristics. As shown in e.g. [2], a second-order lattice Boltzmann scheme which is consistent with the DVBE is given by

$$\bar{f}_i(\mathbf{x}+\boldsymbol{\xi}_i\Delta t,t+\Delta t)-\bar{f}_i(\mathbf{x},t)=-\frac{\Delta t}{\tau+\Delta t/2}\left[\bar{f}_i(\mathbf{x},t)-f^{(0)}(\mathbf{x},t)\right], \tag{3.3}$$

where

$$\bar{f}_i(\mathbf{x},t)=f_i(\mathbf{x},t)+\frac{\Delta t}{2\tau}\left[f_i(\mathbf{x},t)-f_i^{(0)}(\mathbf{x},t)\right].$$

In the simpler and more common scheme used in e.g. [1], $\tau$ is defined differently, so that the fluid becomes inviscid as $\tau\to\frac{1}{2}$ instead of as $\tau\to 0$.

Going from the DVBE in (3.1) to the fully discrete lattice Boltzmann equation in (3.3) introduces a discretisation error, which goes to zero as we increase the numerical resolution. Thus, when studying what the LBM tends towards with increased resolution, we may simply study the DVBE directly.

As the case specified in (2.1) is essentially one-dimensional, we can simulate it with the D1Q3 velocity set, which is the one-dimensional projection of many other common

velocity sets such as D2Q9, D3Q15, D3Q19, and D3Q27. Its velocities are $[\xi_-,\xi_0,\xi_+]=[-1,0,1]\frac{\Delta x}{\Delta t}$, the corresponding weighting coefficients are $[w_-,w_0,w_+]=[\frac{1}{6},\frac{4}{6},\frac{1}{6}]$, and the low-frequency limit of the speed of sound is $c_0=(\frac{\Delta x}{\Delta t})/\sqrt{3}$.

Analogously to (2.1), we assume that the distribution function $\hat{f}_i$ is on phasor form, with an infinitesimal oscillation of amplitude $\hat{f}_i'$ around an equilibrium rest state $F_i^{(0)}$,

$$\hat{f}_i(x,t)=F_i^{(0)}+\hat{f}_i'\,\mathrm{e}^{\mathrm{i}(\omega t-\hat{k}x)}. \tag{3.4}$$

As the velocity $\hat{u}'$ in this case is infinitesimal, (3.2) can be linearised, giving

$$F_i^{(0)}=\rho_0 w_i, \tag{3.5a}$$

$$\hat{f}_i'^{(0)}=w_i\left(\hat{\rho}'+\rho_0\frac{\xi_i\hat{u}'}{c_0^2}\right). \tag{3.5b}$$

By taking the moments of (3.4), we see that this case corresponds to (2.1),

$$\begin{bmatrix}\sum_i(3.4)\\ \sum_i\xi_i(3.4)\end{bmatrix}\quad\Rightarrow\quad\begin{bmatrix}\hat{\rho}(x,t)\\ \rho_0\hat{u}(x,t)\end{bmatrix}=\begin{bmatrix}\rho_0\\ 0\end{bmatrix}+\begin{bmatrix}\hat{\rho}'\\ \rho_0\hat{u}'\end{bmatrix}\mathrm{e}^{\mathrm{i}(\omega t-\hat{k}x)}. \tag{3.6}$$

The pressure can be found from the isothermal equation of state, $p=c_0^2\rho$.

The pressure can also be found in the equilibrium momentum flux tensor [2],

$$\sum_i\boldsymbol{\xi}_i\boldsymbol{\xi}_i(3.2)\quad\Rightarrow\quad\boldsymbol{\Pi}^{(0)}=c_0^2\rho\mathbf{I}+\rho\mathbf{uu}.$$

Analogously, the equilibrium momentum flux of the oscillation in this linearised one-dimensional case becomes

$$\sum_i\xi_i\xi_i(3.5\mathrm{b})\quad\Rightarrow\quad\hat{\Pi}_{xx}'^{(0)}=c_0^2\hat{\rho}'. \tag{3.7}$$

Inserting (3.4) into (3.1), applying the derivatives, and rearranging, we find the harmonic linearised DVBE,

$$[1+\mathrm{i}\tau(\omega-\xi_i\hat{k})]\hat{f}_i'=\hat{f}_i'^{(0)}. \tag{3.8}$$

Because of the $\xi_i$ present in one term, taking any moment of this equation will relate that moment of $\hat{f}_i'$ with its next higher moment. As we shall see, the number of unique moments of $\hat{f}_i'$ is still finite because of the finite number of velocities.

Taking the zeroth, first and second moments of (3.8), we find

$$\frac{\rho_0\hat{u}'}{\hat{\rho}'}=\frac{\omega}{\hat{k}}, \tag{3.9a}$$

$$\frac{\hat{\Pi}_{xx}'}{\rho_0\hat{u}'}=\frac{\omega}{\hat{k}}, \tag{3.9b}$$

$$\hat{\Pi}_{xx}'=\frac{c_0^2\hat{\rho}'+\mathrm{i}\hat{k}\tau\hat{\Pi}_{xxx}'}{1+\mathrm{i}\omega\tau}. \tag{3.9c}$$

With this set of velocities the third moment of $\hat{f}_i'$ is dependent on the first,

$$\hat{\Pi}'_{xxx}=\sum_i \xi_i\xi_i\xi_i\hat{f}_i'=\frac{\Delta x^2}{\Delta t^2}\sum_i \xi_i\hat{f}_i'=\frac{\Delta x^2}{\Delta t^2}\rho_0\hat{u}', \tag{3.10}$$

and the system of moments is closed. Combining Eqs. (3.9) and (3.10), we can find an equation for $\hat{k}$ which is independent of the moments,

$$\left(\frac{\omega}{\hat{k}}\right)^2=\frac{\hat{\Pi}'_{xx}}{\hat{\rho}'}=\frac{1}{1+\mathrm{i}\omega\tau}\left(\frac{c_0^2\hat{\rho}'+\mathrm{i}\hat{k}\tau\frac{\Delta x^2}{\Delta t^2}\rho_0\hat{u}'}{\hat{\rho}'}\right)=\frac{c_0^2+\mathrm{i}\omega\tau\frac{\Delta x^2}{\Delta t^2}}{1+\mathrm{i}\omega\tau}. \tag{3.11}$$

To get this on the form of $\hat{k}/k$ as function of $\omega\tau_\nu$, we first need to express the viscosity number through the shear and bulk viscosities found from the DVBE [2],

$$\left.\begin{aligned}\nu&=\tau c_0^2\\ \nu_B&=2\nu/3\end{aligned}\right\}\quad\overset{(2.5)}{\Rightarrow}\quad \omega\tau_\nu=2\omega\tau. \tag{3.12}$$

Replacing $\frac{\Delta x^2}{\Delta t^2}$ in (3.11) by $3c_0^2$, we can finally rearrange it and find

$$\frac{\hat{k}}{k}=\pm\sqrt{\frac{1+\mathrm{i}\omega\tau}{1+3\mathrm{i}\omega\tau}}=\pm\sqrt{\frac{1+\mathrm{i}\omega\tau_\nu/2}{1+3\mathrm{i}\omega\tau_\nu/2}}. \tag{3.13}$$

The propagation direction is $\pm x$ with the respective choice of sign in (3.13).

Eq. (3.13) was checked against numerical values for the fully discrete LBM. The numerical method previously described in [7] was used to find values in the limit of no discretisation error. The relative difference with (3.13) was on the order of $10^{-11}$, undoubtedly caused by the numerical shortcomings of the previous method. Thus it is clear that sound wave propagation in the LBM tends to (3.13) as we increase the numerical resolution.

It is also possible to find the amplitude ratio and phase shift between the density and momentum waves, as in [7]. This can be done by inserting (3.13) into (3.9a), but this is beyond the focus of this article.

## 4 Comparison with other models

We can now compare the propagation of sound waves as predicted by the DVBE with predictions from other models.

First we should take a closer look at the viscosity number $\omega\tau_\nu$. If $\lambda$ is the wavelength and $l_{\mathrm{mfp}}$ is the mean free path, it can be shown that [12]

$$\left.\begin{aligned}\omega&\sim c_0/\lambda\\ \nu_B\sim\nu&\sim c_0 l_{\mathrm{mfp}}\end{aligned}\right\}\quad\overset{(2.5)}{\Rightarrow}\quad \omega\tau_\nu\sim\frac{l_{\mathrm{mfp}}}{\lambda}=\mathrm{Kn}. \tag{4.1}$$

In words, the viscosity number is essentially the Knudsen number.

The macroscopic behaviour of the Boltzmann equation can be analysed by a multi-scale expansion in Kn, known as the Chapman-Enskog expansion. Truncating to $\mathcal{O}(\mathrm{Kn})$ results in the Navier-Stokes model of the fluid, while truncating to $\mathcal{O}(\mathrm{Kn}^2)$ results in a correction to this, known as the Burnett model [13].

The propagation of sound waves in $+x$ direction in an isothermal monatomic fluid, as given by these models, is

$$\text{Navier-Stokes:} \qquad \frac{\hat{k}}{k}=\frac{1}{\sqrt{1+\mathrm{i}\omega\tau_\nu}}, \tag{4.2a}$$

$$\text{Burnett:} \qquad \frac{\hat{k}}{k}=\frac{\sqrt{2}}{\omega\tau_\nu\sqrt{3}}\sqrt{-1-\mathrm{i}\omega\tau_\nu+\sqrt{1+2\mathrm{i}\omega\tau_\nu+2(\omega\tau_\nu)^2}}, \tag{4.2b}$$

$$\text{DVBE:} \qquad \frac{\hat{k}}{k}=\sqrt{\frac{1+\mathrm{i}\omega\tau_\nu/2}{1+3\mathrm{i}\omega\tau_\nu/2}}. \tag{4.2c}$$

The expressions for Navier-Stokes and Burnett sound propagation are adapted from Greenspan [14], under the isothermal assumption that $\gamma=1$. With this value for $\gamma$, the value of the thermal conductivity can be shown not to affect these acoustic modes. The Burnett expression was found using a binary collision operator with Maxwell molecules, instead of the BGK operator on the RHS of (3.1).

Eqs. (4.2) can be written as series expansions around $\omega\tau_\nu=0$,

$$\text{Navier-Stokes:} \qquad \frac{\hat{k}}{k}=1-\mathrm{i}\frac{1}{2}(\omega\tau_\nu)-\frac{3}{8}(\omega\tau_\nu)^2+\mathrm{i}\frac{5}{16}(\omega\tau_\nu)^3+\frac{35}{128}(\omega\tau_\nu)^4+\cdots, \tag{4.3a}$$

$$\text{Burnett:} \qquad \frac{\hat{k}}{k}=1-\mathrm{i}\frac{1}{2}(\omega\tau_\nu)-\frac{6}{8}(\omega\tau_\nu)^2+\mathrm{i}\frac{20}{16}(\omega\tau_\nu)^3+\frac{308}{128}(\omega\tau_\nu)^4+\cdots, \tag{4.3b}$$

$$\text{DVBE:} \qquad \frac{\hat{k}}{k}=1-\mathrm{i}\frac{1}{2}(\omega\tau_\nu)-\frac{5}{8}(\omega\tau_\nu)^2+\mathrm{i}\frac{13}{16}(\omega\tau_\nu)^3+\frac{139}{128}(\omega\tau_\nu)^4+\cdots. \tag{4.3c}$$

Their terms always alternate between real and imaginary, which means that odd terms in $\omega\tau_\nu$ affect absorption while even terms affect dispersion. The expansions agree to the first order in $\omega\tau_\nu$, but they all disagree at higher orders. Thus, to the lowest order they predict the same absorption but different dispersion.

As the Navier-Stokes model can be found by truncating the Chapman-Enskog expansion to $\mathcal{O}(\mathrm{Kn})$, the model cannot be trusted above this order [12], and it is not surprising that it does not agree with the others at higher orders. That the Burnett and DVBE models disagree at $\mathcal{O}(\mathrm{Kn}^2)$ could also be expected, as the models' transport coefficients depend on the collision mechanism [14]. In this case, where we have two models with two different collision operators, we compare the models by setting their viscosity equal. Any transport coefficients of higher order would be different.

The Navier-Stokes expansion, (4.3a), is a typical binomial series, which converges for $\omega\tau_\nu\leq 1$ and diverges for higher values, even though (4.2a) is valid for any physical (i.e.

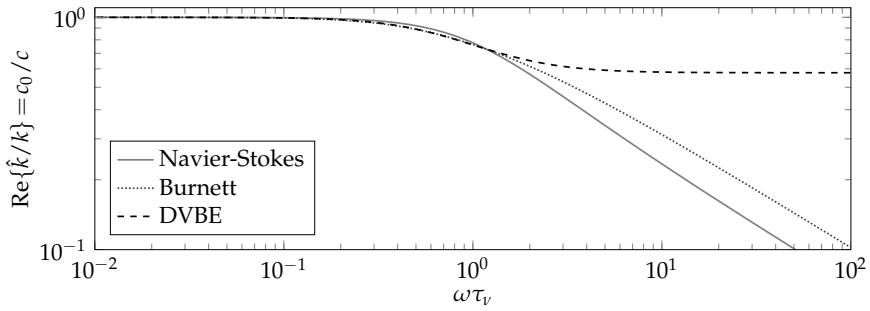


Figure 1: Inverse normalised phase speed in the Navier-Stokes, Burnett, and DVBE models of spatially damped sound waves, against the viscosity number $\omega\tau_\nu$.

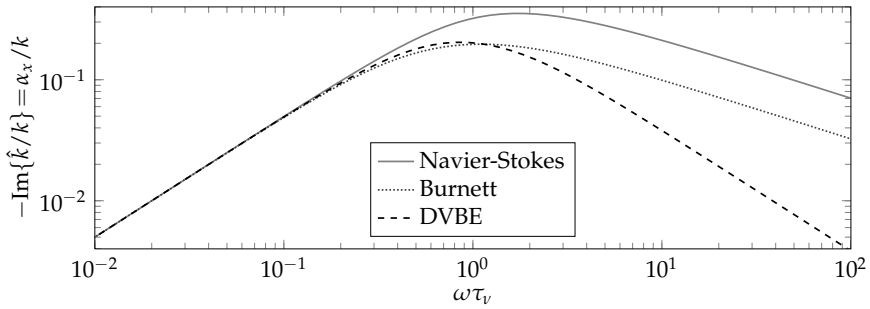


Figure 2: Normalised absorption coefficient in the Navier-Stokes, Burnett, and DVBE models of spatially damped sound waves, against the viscosity number $\omega\tau_\nu$.

real and non-negative) value of $\omega\tau_\nu$. The coefficients in the Burnett and DVBE expansions are never smaller than in the Navier-Stokes expansion for any order, so it is clear by comparison that the convergence ranges of these expansions cannot be larger.

Early approaches to deriving sound propagation from the full Boltzmann equation attacked it by methods of successive approximation [15,16]. They found series like (4.3), which are only useful for small values of $\omega\tau_\nu$. Other approaches have succeeded in finding analytic expressions for dispersion and absorption through different approximations of the Boltzmann equation [13].

We can also use Eqs. (4.2) to graphically compare sound wave propagation in the three models. The dispersion and absorption are shown in Fig. 1 and 2, respectively.

Fig. 1 shows that the DVBE behaves differently to the others at high viscosity numbers, with $c_0/c$ converging towards $1/\sqrt{3}$. This means that $c$ goes to $\frac{\Delta x}{\Delta t}$, the maximum propagation velocity of particles in the D1Q3 velocity set; thus also the information propagation velocity in the model. From this we can expect that extended velocity sets would have different high-frequency behaviour. For the two other models, $c$ goes to infinity with the frequency number, which is clearly unphysical. From high-frequency measurements in argon and air, it has been seen that $c$ plateaus in a similar way to the DVBE [17].

Fig. 2 shows that the absorption has the same kind of behaviour for all three models,

with a peak at $\omega\tau_\nu \sim 1$. The differences lie in the position of the peak and the rate of decline afterwards. The three models have nearly equal behaviour up to $\omega\tau_\nu \sim 0.1$. This indicates that up until this point only the $\mathcal{O}(\omega\tau_\nu)$ term is felt, as the other imaginary terms in the series expansions differ between the models.

In both cases, we see that the three models behave almost identically up to $\omega\tau_\nu \sim 0.1$, and that the DVBE's behaviour is very close to the Burnett model up until about $\omega\tau_\nu \sim 1$, particularly the dispersion. As the Burnett model has been seen to match measurements better than the Navier-Stokes model [14, 17], it seems that the DVBE model captures the viscous effect on sound wave propagation better than the Navier-Stokes model.

## 5 Isotropy in two dimensions

In reality, all simple fluids are isotropic; the behaviour of sound waves is independent of propagation direction. However, any finite discrete set of velocities for the DVBE cannot be isotropic. We will now examine the angular dependence of plane wave propagation with the two-dimensional D2Q9 velocity set. This velocity set is a two-dimensional projection of many three-dimensional velocity sets such as D3Q15, D3Q19, and D3Q27. For one-dimensional behaviour along a main axis, the D2Q9 set itself can be projected down to the D1Q3 set.

Instead of having the wave propagate along the $x$ axis, we now let it propagate at an angle $\varphi$ to this axis. The distribution function is thus generalised from (3.4) to

$$\hat{f}_i(x,y,t) = F_i^{(0)} + \hat{f}_i' \, \mathrm{e}^{\mathrm{i}(\omega t - \hat{k}_x x - \hat{k}_y y)}, \quad \text{where} \quad \hat{k}_x = \hat{k}\cos(\varphi) \quad \text{and} \quad \hat{k}_y = \hat{k}\sin(\varphi). \tag{5.1}$$

The oscillation's equilibrium distribution is also generalised from (3.5b) to

$$\hat{f}_i'^{(0)} = w_i \left[ \hat{\rho}' + \frac{\rho_0}{c_0^2} \left( \xi_{i,x} \hat{u}_x' + \xi_{i,y} \hat{u}_y' \right) \right]. \tag{5.2}$$

The D2Q9 velocity set consists of nine velocities and weighting coefficients,

$$\boldsymbol{\xi}_i = \begin{cases} [0,0], & \text{for } i = 0, \\ \left[\sin(\frac{\pi}{2}[i-1]), \cos(\frac{\pi}{2}[i-1])\right], & \text{for } i = 1,\cdots,4, \\ \left[\sqrt{2}\sin(\frac{\pi}{4}[2i-1]), \sqrt{2}\cos(\frac{\pi}{4}[2i-1])\right], & \text{for } i = 5,\cdots,8, \end{cases} \tag{5.3a}$$

$$w_i = \begin{cases} \frac{4}{9}, & \text{for } i = 0, \\ \frac{1}{9}, & \text{for } i = 1,\cdots,4, \\ \frac{1}{36}, & \text{for } i = 5,\cdots,8. \end{cases} \tag{5.3b}$$

Here we have set $\Delta x = \Delta t = 1$ for notational simplicity. As in (3.13), the final answer will not depend on them. As with the D1Q3 velocity set, the speed of sound is $c_0 = 1/\sqrt{3}$.

We introduce a consistent notation for the moments,

$$\hat{\Pi}'_{x^m y^n} = \sum_i (\xi_{i,x})^m (\xi_{i,y})^n \hat{f}_i'. \tag{5.4}$$

A special notation is used for the case $\hat{\Pi}'_0=\sum_i \hat{f}'_i=\hat{\rho}'$. We have seen earlier that $\hat{\Pi}'_x=\rho_0\hat{u}'_x$, and $\hat{\Pi}'_y=\rho_0\hat{u}'_y$.

With nine velocities there are nine independent moments. Higher moments are dependent on these nine. Similarly to (3.10), we have

$$\begin{aligned}&\hat{\Pi}'_{xxx}=\hat{\Pi}'_x, \quad &&\hat{\Pi}'_{yyy}=\hat{\Pi}'_y, \quad &&\hat{\Pi}'_{xxxy}=\hat{\Pi}'_{xy},\\ &\hat{\Pi}'_{xyyy}=\hat{\Pi}'_{xy}, \quad &&\hat{\Pi}'_{xxxyy}=\hat{\Pi}'_{xyy}, \quad &&\hat{\Pi}'_{xxyyy}=\hat{\Pi}'_{xxy}.\end{aligned} \tag{5.5}$$

From the symmetry properties of the D2Q9 velocity set [11] and (5.2), the moments of the oscillation's equilibrium distribution can be shown to be

$$\hat{\Pi}'^{(0)}_{\alpha\beta}=c_0^2\hat{\Pi}'_0\delta_{\alpha\beta}, \tag{5.6a}$$

$$\hat{\Pi}'^{(0)}_{\alpha\beta\gamma}=c_0^2\left(\hat{\Pi}'_\alpha\delta_{\beta\gamma}+\hat{\Pi}'_\beta\delta_{\alpha\gamma}+\hat{\Pi}'_\gamma\delta_{\alpha\beta}\right), \tag{5.6b}$$

$$\hat{\Pi}'^{(0)}_{\alpha\beta\gamma\delta}=c_0^4\hat{\Pi}'_0\left(\delta_{\alpha\beta}\delta_{\gamma\delta}+\delta_{\alpha\gamma}\delta_{\beta\delta}+\delta_{\alpha\delta}\delta_{\beta\gamma}\right). \tag{5.6c}$$

Here we use Greek letters for arbitrary choices of $x$ or $y$. $\delta_{\alpha\beta}$ is the Kronecker delta.

Putting all of this together, we can find the following system of equations for the nine moments,

$$\begin{bmatrix}1+\mathrm{i}\omega\tau & -\mathrm{i}\hat{k}_x\tau & -\mathrm{i}\hat{k}_y\tau & 0 & 0 & 0 & 0 & 0 & -c_0^4\\ -\mathrm{i}\hat{k}_x\tau & 1+\mathrm{i}\omega\tau & 0 & 0 & -\mathrm{i}\hat{k}_y\tau & 0 & 0 & -c_0^2 & 0\\ -\mathrm{i}\hat{k}_y\tau & 0 & 1+\mathrm{i}\omega\tau & 0 & -\mathrm{i}\hat{k}_x\tau & 0 & -c_0^2 & 0 & 0\\ 0 & -\mathrm{i}\hat{k}_x\tau & 0 & 1+\mathrm{i}\omega\tau & 0 & 0 & -\mathrm{i}\hat{k}_y\tau & 0 & -c_0^2\\ 0 & -\mathrm{i}\hat{k}_y\tau & -\mathrm{i}\hat{k}_x\tau & 0 & 1+\mathrm{i}\omega\tau & 0 & 0 & 0 & 0\\ 0 & 0 & -\mathrm{i}\hat{k}_y\tau & 0 & 0 & 1+\mathrm{i}\omega\tau & 0 & -\mathrm{i}\hat{k}_x\tau & -c_0^2\\ 0 & 0 & 0 & -\hat{k}_y & -\hat{k}_x & 0 & \omega & 0 & 0\\ 0 & 0 & 0 & 0 & -\hat{k}_y & -\hat{k}_x & 0 & \omega & 0\\ 0 & 0 & 0 & 0 & 0 & 0 & -\hat{k}_y & -\hat{k}_x & \omega\end{bmatrix}\begin{bmatrix}\hat{\Pi}'_{xxyy}\\ \hat{\Pi}'_{xyy}\\ \hat{\Pi}'_{xxy}\\ \hat{\Pi}'_{yy}\\ \hat{\Pi}'_{xy}\\ \hat{\Pi}'_{xx}\\ \hat{\Pi}'_y\\ \hat{\Pi}'_x\\ \hat{\Pi}'_0\end{bmatrix}=0. \tag{5.7}$$

As this system becomes too complicated to handle unaided, a computer algebra system was used for the following.

Performing Gaussian elimination on the matrix in (5.7), the last row becomes an equation $g(\hat{k}/k,\omega\tau,\varphi)\,\hat{\Pi}'_0=0$, where the function $g$ is too detailed to fit here. As $\hat{\Pi}'_0\neq 0$ in all cases, we know that $g(\hat{k}/k,\omega\tau,\varphi)=0$. Solving this for $\hat{k}/k$ results in a long, implicit expression which will not fit here either.

However, it is possible to express $\hat{k}/k$ as a series expansion. To the same order as in Eq. (4.3) we find

$$\begin{aligned}\frac{\hat{k}}{k}=1&-\mathrm{i}\frac{1}{2}(\omega\tau_\nu)-\frac{5}{8}(\omega\tau_\nu)^2+\mathrm{i}\frac{13}{16}\left[1+\frac{18}{13}\sin^2(\varphi)\cos^2(\varphi)\right](\omega\tau_\nu)^3\\ &+\frac{139}{128}\left[1+\frac{576}{139}\sin^2(\varphi)\cos^2(\varphi)\right](\omega\tau_\nu)^4+\cdots.\end{aligned} \tag{5.8}$$

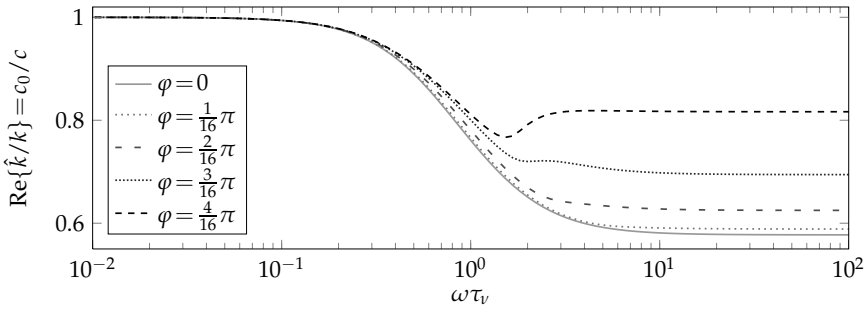


Figure 3: Inverse normalised phase speed in the DVBE model using the D2Q9 velocity set, for spatially damped sound waves propagating at several different angles to the $x$ axis.

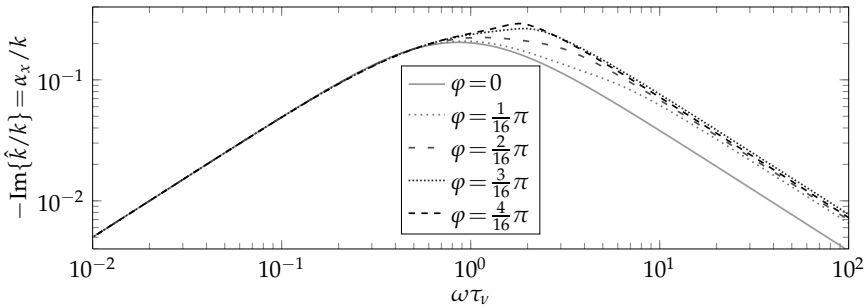


Figure 4: Normalised absorption coefficient in the DVBE model using the D2Q9 velocity set, for spatially damped sound waves propagating at several different angles to the $x$ axis.

We see that the angular dependence starts at $\mathcal{O}(\omega\tau_\nu)^3$. Thus, both dispersion and absorption in the DVBE are isotropic to the lowest order. Also, we can see that (5.8) reduces to (4.3c) at $\varphi = 0$, $\pi/2$, $\pi$, $3\pi/2$; i.e. whenever the propagation direction coincides with a main axis.

It is also possible to find numerical values for $\hat{k}/k$ from given values of $\omega\tau$ and $\varphi$. Figs. 3 and 4 show dispersion and absorption, respectively, against $\omega\tau_\nu$ for several angles $0 \leq \varphi \leq \pi/4$. This angular interval tells us everything about the propagation anisotropy; from (5.8) and the arguments above, it is clearly the angular distance to *any* main axis that affects the propagation. Thus, $\hat{k}/k$ for $0 \leq \varphi \leq \pi/2$ will be mirrored around $\pi/4$. Above $\pi/2$ it will be periodic.

The figures show that there are significant angular variations at $\omega\tau_\nu \sim 1$ and beyond. In particular, we see that the $\omega\tau_\nu \to \infty$ limit of $c$ is $\cos(\varphi)$ for $0 \leq \varphi \leq \pi/4$. At $\pi/4$, when the sound propagates parallel to the diagonal particle velocities, the speed of sound is half of the diagonal particle speed. The absorption still behaves qualitatively the same for any angle, although for propagation not along the main axis the peak is positioned elsewhere and is somewhat uneven.

Even so, we see that the sound wave propagation in the DVBE model, using the D2Q9 velocity set, is practically isotropic up to about $\omega\tau_\nu \sim 0.1$. Thus, anisotropy of the viscous

effects in LBM simulations can be made negligible at audible frequencies by improving the numerical resolution.

## 6 Conclusion

The discrete-velocity Boltzmann equation is a limiting case of the lattice Boltzmann method. As the numerical resolution is improved, the LBM tends towards the DVBE. From the DVBE we found Eq. (3.13) which describes the absorption and dispersion of sound waves propagating along a main axis, for any velocity set that can be projected down to D1Q3.

The DVBE model is reminiscent of the approach taken by Grad to find the 13-moment model [18]. Since taking any moment of the Boltzmann equation results in an equation coupling a particular moment of $f$ with its next higher moment, the Boltzmann equation is equivalent to an infinite system of equations coupling an infinite number of moments. Grad solved this problem by keeping the moments needed for the system to contain the Navier-Stokes model as an approximation, and simply setting the rest to zero. For sound propagation, the Grad-13 model agrees with the Burnett model to $\mathcal{O}(\mathrm{Kn}^2)$ when the models are based on the same collision operator [14]. In the DVBE model, the system of moments is also closed, as sufficiently high moments are given by lower ones. However, this happens as a consequence of the finite velocity set; only the choice of the velocity set determines how the system of equations is closed.

The sound wave propagation found for the DVBE with the D1Q3 velocity set was compared to similar expressions from the Navier-Stokes and Burnett models. The agreement is good up to $\omega\tau_\nu \sim 0.1$. Above this, all three models increasingly disagree. However, all three models can be seen as different approximations to the Boltzmann equation. Of the Navier-Stokes and Burnett models, the latter gives the best match with both the DVBE and measurements [14, 17]. (It is not possible to compare this DVBE model directly to measurements, as it simulates an unphysical isothermal gas.) Additionally, the DVBE alone qualitatively captures the phase speed plateau seen in high-frequency experiments [17]. In the other models, the phase speed goes unphysically to infinity with the frequency.

The D2Q9 velocity set was used to examine the isotropy of the DVBE for a plane sound wave propagating at an angle to the $x$ axis. We saw that absorption and dispersion were angle-independent to the lowest order in the expansion. There was no significant dependence on angle up to $\omega\tau_\nu \sim 0.1$. At high frequencies, the phase speed plateaus at different values, whereas the absorption goes towards zero for all angles.

To summarise these results, the behaviour of the DVBE is sufficiently correct up to $\omega\tau_\nu \sim 0.1$. By extension, the LBM can be made to be as correct by improving the numerical resolution. In gases, the quantity $\tau_\nu$ tends to be on the order of $10^{-10}$ s [19]. This indicates that the DVBE gives a very good description of an isothermal gas up to frequencies of the order $10^8$ Hz. For comparison, the upper limit of human hearing is commonly specified as

$2\times10^4$ Hz. Thus, any errors in the DVBE are negligible when simulating audible sound.

Even though we have seen that the DVBE model agrees with the others up to very high frequencies, the isothermal gas which it simulates is quite artificial. Thermal conduction does have a significant effect on sound wave absorption in gases.

Still, in cases where conduction does not affect the flow significantly, the contribution from thermal conduction to absorption can be simulated to the lowest order by increasing the bulk viscosity artificially [9]. There exist extensions to the LBM that allow setting the bulk viscosity arbitrarily [2, 20]. This would also affect the other sound wave properties: The amplitude ratio and phase shift between the density and momentum wave fields, and the dispersion. However, these properties may usually be considered less physically significant than the absorption, and the dispersion and amplitude ratio already disagree with theory to the lowest order in $\omega\tau_\nu$ [7].

In the audible range in air, relaxation between translational energy and vibrational energy in $N_2$ and $O_2$ is very important. It gives a contribution to the absorption of sound waves which can be several magnitudes stronger than the combined effect of viscosity and conduction [9, 19]. How this mechanism may be implemented in the lattice Boltzmann method remains to be seen.

## Acknowledgments

The author would like to thank Paul J. Dellar for several comments which were invaluable to the writing of this article.

### References

[1] S. Chen and G. D. Doolen, Lattice Boltzmann method for fluid flows, Annu. Rev. Fluid Mech., 30 (1998), 329–364.
[2] P. J. Dellar, Bulk and shear viscosities in lattice Boltzmann equations, Phys. Rev. E, 64 (2001), 031203.
[3] M. Hasert, J. Bernsdorf, and S. Roller, Towards aeroacoustic sound generation by flow through porous media, Phil. Trans. R. Soc. A, 369 (2011), 2467–2475.
[4] A. Wilde, Calculation of sound generation and radiation from instationary flows, Comput. Fluids, 35 (2006), 986–993.
[5] M. J. Lighthill, On sound generated aerodynamically I. General theory, Proc. R. Soc. A, 211 (1952), 564–587.
[6] M. Popescu, S. T. Johansen, and W. Shyy, Flow-induced acoustics in corrugated pipes, Commun. Comput. Phys., 10 (2011), 120–139.
[7] E. M. Viggen, Viscously damped acoustic waves with the lattice Boltzmann method, Phil. Trans. R. Soc. A, 369 (2011), 2246–2254.
[8] Y. Li and X. Shan, Lattice Boltzmann method for adiabatic acoustics, Phil. Trans. R. Soc. A, 369 (2011), 2371–2380.
[9] D. T. Blackstock, Fundamentals of Physical Acoustics, Ch. 9, John Wiley & Sons, 2000.

[10] C. Truesdell, Precise theory of the absorption and dispersion of forced plane infinitesimal waves according to the Navier-Stokes equations, J. Rational Mech. Anal., 2 (1953), 643–730.
[11] J. Latt, Hydrodynamic limit of lattice Boltzmann equations, Ch. 2, PhD Thesis, University of Geneva, 2007.
[12] J. Foch and G. E. Uhlenbeck, Propagation of sound in monatomic gases, Phys. Rev. Lett., 19 (1967), 1025–1027.
[13] P. J. Dellar, Macroscopic descriptions of rarefied gases from the elimination of fast variables, Phys. Fluids, 19 (2007), 107101.
[14] M. Greenspan, Transmission of sound waves in gases at very low pressures, in Physical Acoustics IIA, Academic Press, 1965.
[15] C. S. Wang Chang and G. E. Uhlenbeck, The kinetic theory of gases, in Studies in Statistical Mechanics V, North-Holland Publishing Company, 1970.
[16] J. Foch and G. W. Ford, The dispersion of sound in monatomic gases, in Studies in Statistical Mechanics V, North-Holland Publishing Company, 1970.
[17] E. Meyer and G. Sessler, Schallausbreitung in Gasen bei hohen Frequenzen und sehr niedrigen Drucken, Z. Phys., 149 (1957), 15–39.
[18] H. Grad, On the kinetic theory of rarefied gases, Comm. Pure Appl. Math., 2 (1949), 331–407.
[19] L. E. Kinsler, A. R. Frey, A. B. Coppens, and J. V. Sanders, Fundamentals of Acoustics, John Wiley & Sons, 2000.
[20] S. Bennett, A lattice Boltzmann model for diffusion of binary gas mixtures, Ch. 4, PhD Thesis, University of Cambridge, 2010.